A Fluidic Soft Robot for Needle Guidance and Motion Compensation in Intratympanic Steroid Injections

Lukas Lindenroth, *Member, IEEE*, Sophia Bano, Agostino Stilli, *Member, IEEE*, Joseph G. Manjaly, and Danail Stoyanov, *Senior Member, IEEE*

***Abstract*—Intratympanic steroid injections are commonly employed in treating ear diseases, such as sudden sensorineural hearing loss or Meniere's disease through drug delivery via the middle ear. Whilst being an effective treatment, the procedure has to be performed by a trained surgeon to avoid delicate regions in the patient's anatomy and is considered painful despite the use of topical anaesthesia. In this letter we introduce a fluid-driven soft robotic system which aims at increasing patient-comfort during the injection by counteracting unwanted needle motion, reducing the cognitive load of the clinician by autonomously identifying sensitive regions in the ear and de-risking the procedure by steering the needle towards the desired injection site. A design comprising of six embedded fluidic actuators is presented, which allow for translation and rotation of the needle as well as adaptive stiffening in the coupling between needle and ear canal. The system's steering-capabilities are investigated and the differential kinematics derived to demonstrate trajectory tracking in Cartesian space. A vision system is developed which enables tracking of anatomical landmarks on the tympanic membrane and thus locating the desired needle insertion site. The integrated system shows the ability to provide a safe guide for the inserted needle towards a desired target direction while significantly reducing needle motion. The proposed tracking algorithm is able to identify the desired needle insertion site and could be employed to avoid delicate anatomical regions.**

***Index Terms*—Computer vision for medical robotics, medical robots and systems, soft robotics applications.**

Manuscript received October 15, 2020; accepted December 17, 2020. Date of publication January 14, 2021; date of current version February 3, 2021. This letter was recommended for publication by Associate Editor Kirstin Hagelskjaer Petersen and Kyu-Jin Cho upon evaluation of the reviewers' comments. This work was supported by the Wellcome/EPSRC Centre for Interventional and Surgical Sciences (WEISS) at UCL (203145Z/16/Z), EPSRC (EP/P027938/1, EP/R004080/1), The work of D. Stoyanov is supported by a Royal Academy of Engineering Chair in Emerging Technologies (CiET1819_2_36) and an EPSRC Early Career Research Fellowship (EP/P012841/1). *(Corresponding author: Lukas Lindenroth.)*

Lukas Lindenroth, Sophia Bano, Agostino Stilli, and Danail Stoyanov are with the Wellcome/EPSRC Centre for Interventional and Surgical Sciences, University College London, London W1W 7EJ, U.K. (e-mail: l.lindenroth@ucl.ac.uk; sophia.bano@ucl.ac.uk; a.stilli@ucl.ac.uk; danail.stoyanov@ucl.ac.uk).

Joseph G. Manjaly is with the National Institute for Health Research, University College London Hospitals Biomedical Research Centre Deafness and Hearing Problems Theme, Ear Institute, University College London, WC1X 8DA, U.K. and the Royal National ENT & Eastman Dental Hospitals, University College London Hospitals, London WC1E 6DG, U.K. (e-mail: joseph.manjaly@nhs.net).

Digital Object Identifier 10.1109/LRA.2021.3051568

I. Introduction

THE World Health organisation estimates that hearing loss affects 500 million people worldwide, with far reaching social, educational and economic consequences where sensorineural hearing loss makes up around 90% of this burden [1]. The anatomical location of the cochlear within dense bone makes it an isolated organ. Low blood flow to the cochlear and a limited blood-labyrinth barrier are the reasons development of systemic therapies for inner ear disorders has not yet yielded great success [2], [3]. Intracochlear drug delivery via a surgical route offers the highest concentration of drug delivery, but at present is associated with a highest risk of diminishing hearing, making it only suitable in pre-existing profound losses.

Drug delivery to the inner ear via diffusion from the middle ear is therefore the most attractive option. Intratympanic injection of steroids is a first-line treatment option for both sudden sensorineural hearing loss and Meniere's disease [2], [3]. This delivery method is also the focus for development of novel therapeutics. Drugs delivered in this way can bypass the blood-perilymph barrier and deliver higher local concentration for drugs that have narrow therapeutic window or serious side effects. Interest in this field has been increasing rapidly, with an ever-increasing number of therapeutic development programmes around the world progressing along the translational pathway. Clinical trials of otoprotective, restorative and regenerative therapeutics are underway with several being in advanced stages of clinical trials [4].

Currently intratympanic injections are only delivered by experienced ear, nose and throat (ENT) surgeons. This will become a limiting step should a widely indicated inner ear therapeutic come to market for reversal of sensorineural hearing loss. "De-risking" the procedure to enable safe delivery by non-surgeons involves a number of considerations. The procedure can be painful for patients. This may be related to needle movement within the tympanic membrane. The delivering clinician requires a steady hand and the ability to respond in real-time to patient movement. There is a risk of damage to middle and inner ear structures by incorrect needle placement leading to dead hearing, vertigo and tinnitus. Portability and delivery outside the hospital environment is also a factor with the current delivery technique also requiring a full otologic microscope which requires room space.

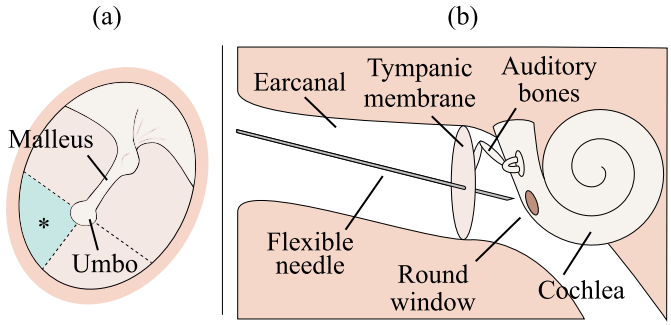

Fig. 1. View of the tympanic membrane with umbo and malleus with the posteroinferior quadrant (*) (a) and intratympanic steroid delivery to the round window of the cochlea (b).

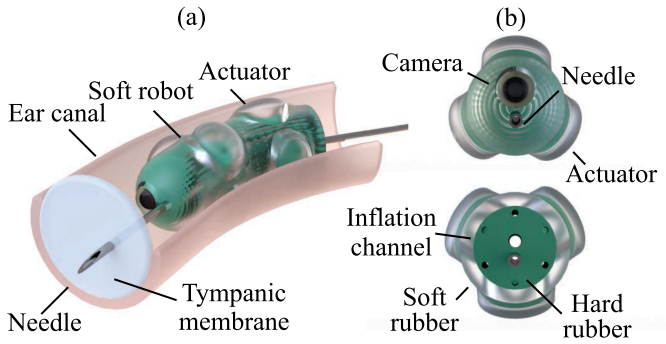

Fig. 2. Conceptual drawing of the proposed soft robotic system for intratympanic injections within a patient's ear canal (a) and cross-sectional view (b).

Targeted diagnosis, drug delivery and surgery within natural orifices has been increasingly adopted in recent years [5]. Handling tools within natural orifices, however, is considered difficult, as for example seen when comparing natural orifice transluminal endoscopic surgery (NOTES) with conventional laparoscopic surgery [6]. Hence, providing active robotic assistance in guiding instruments safely within a patient's lumen could reduce both cognitive and physical workloads on the surgeon, presumably leading to reduced risk and discomfort for the patient.

In the context of endoluminal procedures several robotic systems have been developed to overcome the lack of dexterity of traditional scopes and tools. To perform endoluminal navigation these continuum systems are typically pushed by the user from their base through the targeted orifice. Given the wide range of deadly pathologies associated with the gastro-intestinal tract [7] and the clinical need for better screening tools, in the context of endoluminal procedures research effort has focused significantly on the development of dexterous devices for gastroscopy and colonoscopy. Continuum designs such as the flexible tendon-driven system presented in [8] have been widely explored in medical research. A number of these systems have been successfully translated into medical products with the NeoGuide Endoscopy System (NeoGuide Endoscopy System Inc., Los Gatos, CAUSA), the Invendoscope ^{TM} SC40 (Invendo Medical GmbH, Weinheim, Germany) and the ColonoSight (Stryker GI Ltd., Haifa, Israel) [9] amongst others.

In the endoluminal scenario the morphology of the lumen can be leveraged to enhance the navigation and the imaging capabilities of the deployed system by directly interacting with the environment. For example the Soft pneumatic inchworm Double balloon (SPID) for colonoscopy system [10] makes use of a set of two inflatable actuators in combination with a 3-DOF Soft Pneumatic Actuator (SPA) to provide propulsion, camera steering and stabilization. A similar locomotion principle has been explored in [11] where a self-propelled soft robotic system based on shape-memory alloy (SMA) springs is proposed. In this case the alternation between extension and compression of the internal spring elements results in a local radial and axial deformation of a specific segment of the system. This motion sequence leads to local interactions between the walls of the lumen and the deformable elements of the system, providing both propulsion and camera stabilization.

Soft robotic design solutions have been extensively investigated in the context of endoluminal robotic systems because the use of compliant materials like silicone can significantly reduce the risk of damage to the walls of the navigated lumen, while providing adaptability to different lumen geometries. The ability to adapt to the lumen geometry as well as being able to anchor to its walls is also highly beneficial to the quality of the images acquired and clearly a feature sought by clinical experts, as the development and translation into a clinical product of the Aer-O-Scope System (GI View Ltd., Ramat Gan, Israel) [12], a flexible colonoscope embedding multiple inflatable elements, has shown.

Whilst robotic and in particular soft robotics systems and medical devices aiming at a variety of endoluminal procedures exist, the ear presents a new challenge due to its small diameter, highly non-uniform shape and fragility. Soft robotics can, with its high potential for scalability, its inherent safety and adaptability potentially provide an efficient way for aiding in intratympanic steroid injections. In this work we propose a soft robotic system that assists in intratympanic needle guidance by being able to

- actively steer inside a lumen to guide a needle towards a desired point of injection on the tympanic membrane;
- compensate hand motion of the operating surgeon by providing actively controllable mechanical coupling between needle and the patient's ear canal;
- autonomously identify a desired site for intratympanic injection according to anatomical priors.

II. Methods

As part of intratympanic steroid injections the patient is placed in a supine position and topical anaesthetic is applied to the tympanic membrane under otoscope guidance. Once the needle is inserted into the membrane, as shown in Fig. 1 b), the viscous steroid gel is injected. The patient then remains idle for a short period to prevent the gel from dispersing. Steroid gel is injected with the aim to perfuse via the round window membrane on the cochlea into the inner ear. As the view onto the round window is obstructed by the tympanic membrane, assumptions have to be made about the location of the round window. The tympanic membrane is commonly divided into quadrants according to the visible middle ear anatomy. The

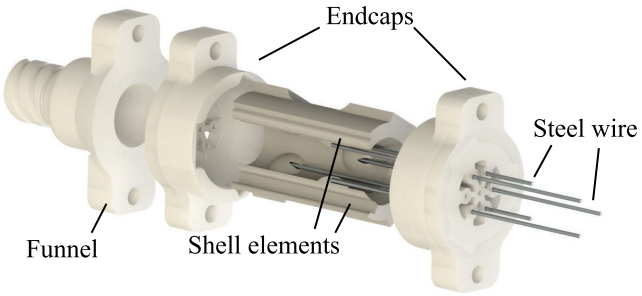

Fig. 3. First of two injection moulds required for fabricating the proposed soft robot.

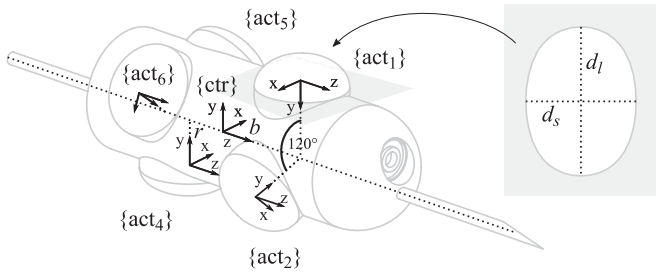

Fig. 4. Freebody diagram of the soft robot with actuator reference frames $\{\text{act}_i\}$, robot centre $\{\text{ctr}\}$ and actuator cross-section.

malleus serves as a principle axis of this division and the umbo indicates the intersection with the second axis, dividing the tympanic membrane into four quadrants. It is commonly assumed that the posteroinferior quadrant of the tympanic membrane enables the desired approach angle towards round window and as such employed as a reference landmark in this study.

Assuming the injection needle used during the procedure is inserted manually through the robot, compensation of the clinician's hand motion to reduce discomfort during the procedure can be achieved in at least two ways. Firstly, a mechanical fixture could be employed to stabilise the patient's head and provide a feeding guide for the needle, thus linking the two to a single external mechanical reference. Whilst this is common practice in e.g. brain surgery, the here-addressed procedure is highly outpatient-centric and thus clamping would be impractical.

Secondly, an alternative to coupling patient and tool to an external reference is to link needle and patient directly. Mechanisms to provide elastic contacts between surgical tools and a surrounding lumen exist and are most prominently applied in vascular surgery, but also find applications in other ENT procedures such as balloon dilation for sinusitis and eustachian tube dysfunction, as seen e.g. in the ACCLARENT AERA$^{\text{TM}}$ system (Acclarent, USA). As such devices inflate predominantly radially around a central tool, steering of the tool is only possible externally. Directed, differential control could be achievable in case of a compartmentalised balloon.

A robotic system to address this procedure is at the minimum required to provide the necessary degrees of freedom to steer the needle to the desired injection site. This includes translation motion in a plane parallel to the tympanic membrane as well as rotation around these axes. In this investigation, needle insertion is assumed to be performed manually by the operating clinician and hence this DOF is ignored. Rotation around the long axis of the needle is ignored due to axial symmetry, thus yielding a total of four required spatial DOFs. Given the endoluminal nature of the system, the view of the tympanic membrane from outside the ear canal would be obstructed. Hence, an integrated endoscopic camera system to provide close-up feedback of the tympanic membrane would be desired.

A. System Design and Fabrication

In this work we make use of the inherently compliant nature of soft robotic systems to provide a coupling and steering mechanism for intratympanic needle insertion. The system is comprised of a cylindrical silicone rubber body which is formed of a stiff core which is overmoulded by a softer membrane, as shown in Fig. 2a). Inflatable actuation chambers are distributed radially in two parallel planes, which will be referred to as actuation stages. For the given design, six chambers are arranged in two actuation stages which comprise of three radially-aligned actuation chambers each, as shown in Fig. 2b). This allows for translation when both stages are actuated in the same manner, rotation if actuated differentially as well as any combination of the four DOFs. The redundancy in both actuation stages enable simultaneous inflation and thus radial expansion of the device, which allows for controlling the coupling pressure between robot and lumen and thus countering external disturbances such as hand motion during the needle insertion.

The actuation stages are rotated at 180° with respect to one another which allows for straight routing of the fluid channels without intersecting other actuators. A central channel allows for feeding the needle to the desired target. The envisioned design can function given that the core material is significantly stiffer than the surrounding rubber, thus prevention collapsing of the fluid channels and needle guide.

Fabrication of the prototype is achieved in a two stage process. Initially the core is moulded using the injection mould shown in Fig. 3. The mould shell elements comprise of nodules in the locations of the desired fluid actuators. The nodules are linked to one end of the mould with steel wire (ø0.5 mm), which forms the fluid channels directing working fluid to the actuators. Liquid rubber is injected through the bottom funnel. In the second stage of the process the core is overmoulded using a softer rubber. Cavities in the core element, which are caused by the shell nodules and later form the inflatable actuators, are retained with the help of gel wax to block silicone rubber injected in the second layer. The gel wax is inserted manually and heated to fill the cavities up to the surface of the core. Once the second layer of rubber is fully cured, the gel wax in the actuation chambers is melted and removed by flushing the chambers repeatedly with hot water. In this work, two variations of the design are employed. The first only comprises of a single central channel which serves as the needle guide. The second contains both an off-centre needle channel as well as a miniature camera.

The proposed fabrication pipeline enables efficient scaling of the resulting robot beyond the envisioned application. In this work, the soft robot is dimensioned at twice the scale expected

for the given application to allow for integration of a miniature camera. The human ear canal is on average ≈7 mm in diameter and ≈25 mm in length [13]. Hence, the dimensions of the scaled up robot are 8 mm in diameter and 20 mm in length to allow for sufficient space to steer inside the lumen. The fluid actuator cross-section is chosen to cover a sufficiently large surface area without intersecting the surrounding fluid channels. The projection of the actuators is of quasi-elliptical shape, with a long axis d_l of 4.9 mm and a short axis d_s of 3.63 mm, as shown in Fig. 4. At the actuator centerpoint they comprise of a depth of 1.25 mm between core and outer membrane. The outer soft membrane layer is of 1 mm thickness.

B. Differential Kinematics

The robot's differential kinematics are obtained from the wrenches induced by the inflating actuation chambers. An overview of the corresponding reference frames is shown in Fig. 4.

Upon inflation, a single actuation chamber i in contact with a surrounding lumen induces a radial force $f_{act,i}$ acting on the core element of the robot. The exerted force induces a wrench $\boldsymbol{w}_{ctr}$ in the centre of the robot $\{\text{ctr}\}$ such that

$$\boldsymbol{w}_{ctr} = \boldsymbol{Ad}_{act,i} \cdot \boldsymbol{w}_{act,i} \tag{1}$$

With the local wrench induced by actuation chamber i $\boldsymbol{w}_{act,i} = [0, f_{act,i}, 0, 0, 0]^T$ and the wrench transformation matrix $\boldsymbol{Ad}_{act,i}$. The latter can be obtained assuming a rigid transformation between local frame $\{\text{act}_\text{i}\}$ and robot centre frame.

The actuation matrix $\boldsymbol{H}$ of a system comprising of n actuators can be defined as

$$\boldsymbol{H} = [\boldsymbol{Ad}_{2,1}, \ldots, \boldsymbol{Ad}_{2,n}] \tag{2}$$

Where $\boldsymbol{Ad}_{2,i}$ is the second column of the wrench transformation corresponding to actuator i. The inverse Jacobian is then defined such that

$$\boldsymbol{J}^{-1} = \boldsymbol{H}^T \tag{3}$$

For the given system, the inverse Jacobian of the system $\boldsymbol{J}^{-1} \in 6 \times 4$ can be defined as

$$\boldsymbol{J}^{-1} = \begin{bmatrix} 0 & -1 & b & 0 \\ \frac{\sqrt{3}}{2} & \frac{1}{2} & -\frac{1}{2}b & \frac{\sqrt{3}}{2}b \\ -\frac{\sqrt{3}}{2} & \frac{1}{2} & -\frac{1}{2}b & -\frac{\sqrt{3}}{2}b \\ 0 & 1 & b & 0 \\ -\frac{\sqrt{3}}{2} & -\frac{1}{2} & -\frac{1}{2}b & \frac{\sqrt{3}}{2}b \\ \frac{\sqrt{3}}{2} & -\frac{1}{2} & -\frac{1}{2}b & -\frac{\sqrt{3}}{2}b \end{bmatrix} \tag{4}$$

Where b is the distance between soft robot centre and actuation stage. It can then be employed to solve the inverse differential kinematics of the system as

$$\delta \boldsymbol{q} = \boldsymbol{J}^{-1} \cdot \delta \boldsymbol{X} \tag{5}$$

Where $\delta \boldsymbol{X} = [\delta_x, \delta_y, \theta_x, \theta_y]^T$ is the relative pose change of the robot in the centre frame and $\delta \boldsymbol{q}$ the respective actuation chamber inflation. $\boldsymbol{q}$ is mapped linearly to the induced fluid volumes $\boldsymbol{V}$. The relationship is found experimentally. The global pose of the system can be obtained through integration.

Whilst this approach accounts for the directional decomposition of the actuator motion, it ignores actuator compliance and changes in its expansion configurations.

C. Vision

The desired needle insertion point is defined as the centre of the posteroinferior quadrant of the tympanic membrane. The exact location in the image is obtained by identifying surrounding anatomical landmarks. Anterior and posterior quadrants are differentiated by the centerline of the malleus, whilst inferior and superior are separated by a perpendicular axis intersecting the previous at the centerpoint of the umbo. Thus, the relevant quadrant can be deduced from the locations of the tympanic membrane, malleus and umbo. This requires establishing machine intelligence to recognise the anatomical landmarks.

The landmarks localisation problem is formulated as a semantic segmentation task that involves pixel-wise labelling of an image. Semantic segmentation is a highly researched topic in Computer Vision with several deep learning-based solutions already proposed [14]. Since DeepLabV3+ [15] has outperformed several state-of-the-art segmentation networks, we deployed this network for classifying each pixel in an image into the background, tympanic membrane, malleus and umbo. DeepLabV3+ combines spatial pyramid pooling with encoder-decoder structure as a result it allows multi-scale contextual information encoding through atrous convolutions at different dilation rates. The gradual recovery of the spatial information is achieved through a simple decoder that allows capturing sharper object boundaries. We used MobileNetV2 [16] as the backbone which is lightweight and robust for mobile applications. We refer to [15], [16] for specific details about the network architectures.

For training the segmentation model, pixel-wise annotations of 277 tympanic membrane images of 500×500 resolution (obtained from [17]) are performed to obtain the ground-truth (GT) segmentation masks. To capture the domain variability when steering the robot in the ear canal, an additional set of 80 images of resolution 640×480 pixels are acquired through steering a camera (Digital Otoscope, Jiusion, U.K.) in medical training ear phantom and pixel-wise annotating these images (details in Sec. II-D4). The DeepLabV3+ model is trained using 216 tympanic membrane and 60 phantom images, while the remaining images are used for testing. The fitted miniature camera (MD-V1001L-91X, Misumi Electronics Corporation, Taiwan) in the final experimental setup is of 200×200 of pixel resolution having heavy RGB colour shift. As a result, the trained network may end up with inaccurate results due to training data distribution being significantly different from the test data distribution. To overcome this issue, data augmentation is applied that included applying scale, rotation and perspective transforms, horizontal and vertical flips, RGB colour shifts, brightness, contrast, saturation and blurring operations at random with a probably of 0.5 during the training process. Adam optimiser is used with a learning rate of 0.001. The network is trained for

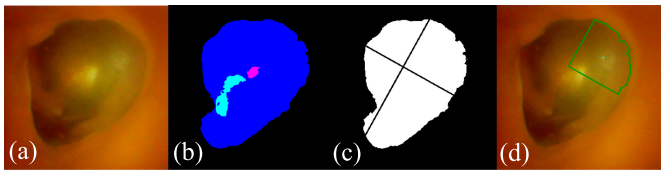

Fig. 5. Overview of the proposed vision algorithm with the original image (a), the predicted segmentation (b) of tympanic membrane (blue), umbo (green) and malleus (red), the calculated quadrant mask (c) and the final insertion point location on the tympanic membrane (d).

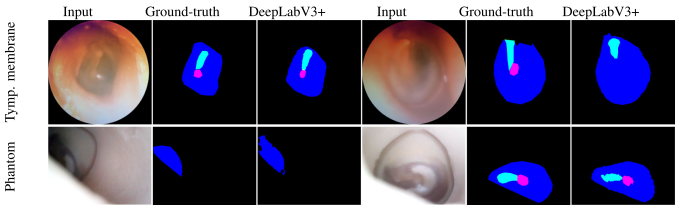

Fig. 6. Anatomical landmarks segmentation results. (Top-right) Umbo is missed by the network since it is not visible in the input image. (Bottom row) Examples from phantom test where landmarks are partially visible.

300 epochs with early stopping on a Tesla V100-DGXS-32 GB GPU (Nvidia Corporation, Santa Clara, CA, US).

Intersection over Union (IoU) is a standard performance metrics for segmentation evaluation that quantifies the overlap between the GT and predicted masks, where a value close to 1 suggests high overlap. We obtained a mean IoU of 0.80 on the hold-out test tympanic membrane and phantom images which shows the robustness of the model. The qualitative results on the test images are shown in Fig. 6. During real-time tracking, this trained model is used for automatic segmentation of the anatomical regions. A line fitted through the segmented region of the malleus specifies the first principle axis. The second axis is perpendicular to the first and intersecting at the point of shortest distance between the first axis and the centre of the segmented umbo. According to this calculation a mask is created to determine the four quadrants (Fig. 5c)). The needle insertion site is then calculated as the centre of the intersection between the segmented tympanic membrane and defined posteroinferior quadrant (Fig. 5d)).

D. Experimental Validation

Experimental setups are created to determine the steering capabilities of the proposed design, its ability to counteract undesired needle motion and its targeting capabilities. Three robot prototypes are created for which the outer rubber materials are varied between Ecoflex 00-30 (EF30), Ecoflex 00-50 (EF50) and Dragon Skin Fx Pro (DSFX) (Smooth-On Inc., Pennsylvania, USA). Platinum-cured silicone rubber tubing (0.5 mm ID and 1 mm OD) is connected through short needle segments which are inserted into the dilated fluid channels. For all prototypes the core material is Smooth-Sil 960 (Smooth-On Inc., Pennsylvania, USA). Actuation fluid is provided through stepper motor-driven syringe pumps which have first been shown in previous research [18]. The pumps are equipped with 3 ml syringes and

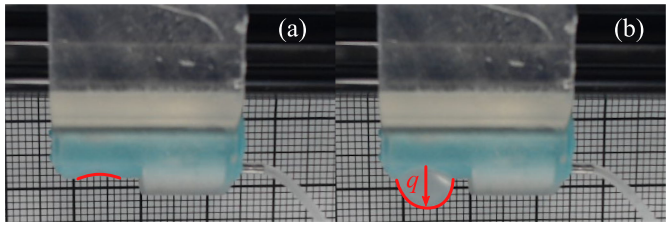

Fig. 7. Actuation chamber inflation for 0% (a) and 75% (b) of the maximum actuation fluid volume.

motion commands are generated by a six-axis motion controller (TMCM-6214, Trinamic GmbH, Germany) which is interfaced with a host PC running ROS. Deionized water is used as a working fluid.

1) Actuation Characteristics: The actuation behaviour of the system is investigated by introducing working fluid into the actuator chambers and measuring the radial inflation distance q. For this purpose the soft robot is aligned with the direction of actuation perpendicular to the image plane of a camera. Images are obtained using a camera (C922, Logitech, Switzerland) under increasing fluid volume V. This is repeated for all six actuation chambers of the robot. The radial inflation q of the actuators is determined manually from the furthest distance between actuator and baseline at 0% inflation. A visual comparison for different inflation levels in presented in Fig. 7.

2) Steering Capabilities: To determine the robot's ability to steer an inserted needle inside a lumen, it is placed inside an acrylic tube (14 mm ID) to simulate a simplified ear canal at twice the average diameter of 7mm [13]. Initially, all actuators are inflated by an offset volume to align the robot with the lumen centre. While maintaining stable contact, trajectories are defined according to the differential kinematics defined in 5. Desired motions are defined as linear and circular trajectories in Cartesian space in position and orientation. The resulting motion is measured by an electromagnetic (EM) tracker Aurora (Northern Digital Inc., Waterloo, Canada) which is manually aligned and inserted into the robot's central channel.

3) Motion Compensation: To determine the robot's motion compensation capabilities, it is placed in the configuration described in Section II-D2. A needle (Spinal needle 27 G, Vygon, France) is inserted into the central channel of the soft robot with the needle base being affixed to a robotic manipulator (UR3, Universal Robots, Odense, Denmark). The latter generates a defined displacement at the needle base. An EM-tracker is attached to the distal end of the needle to measure the needle tip displacement relative to the manipulator's motion, which is validated for increasing fluid levels. The experimental setup is shown in Fig. 8.

4) Target Identification and Tracking: The proposed vision system is trialled in identifying and tracking the desired needle insertion point as described in Sec. II-C. This is achieved by positioning the employed camera (MD-V1001L-91X, Misumi Electronics Corporation, Taiwan) using a robotic manipulator over a printout of one of three images of the tympanic membrane as taken from [17]. Three images with decreasing difficulty are chosen according to some qualitative preliminary evaluation.

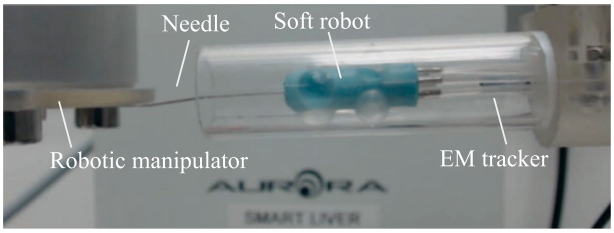

Fig. 8. Motion compensation experiment with a robotic manipulator inducing needle motion recorded by an EM tracker.

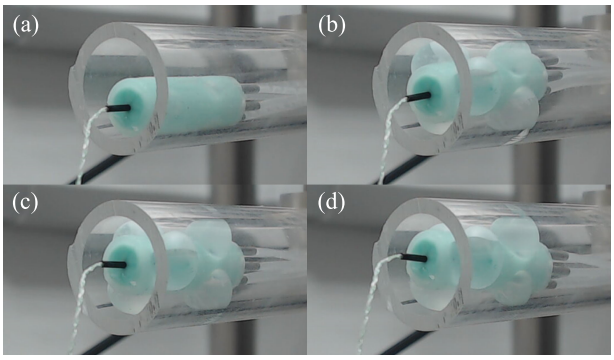

Fig. 9. Subset of soft robot motions achievable within a cylindrical lumen. The deflated robot (a) is inflated by an offset volume to center itself within the lumen (c). Independent actuator inflation then allows for steering, such as a down- (b) and up-tilt (d).

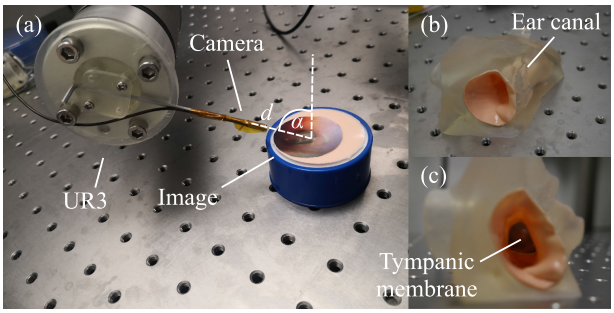

Fig. 10. Validation experiment to assess target tracking in stationary views for varying tilt angle α and target distance d (a) and phantom to trial robot insertion into the ear canal with image feedback (b-c) given a patient-specific model.

The images are taken at a defined distance d and angle between camera plane and image plane α. The proposed target detection algorithm is run for 100 samples and variability in the target point is determined. The experimental setup is shown in Fig. 10a).

Tracking of the target is validated by integrating the camera in the soft robot and steering it within a custom phantom. It is designed around patient-specific CT models available through the openEAR library [19]. A single patient model is selected (patient *alpha*) and adapted to hold the image of a tympanic membrane. The model is 3d-printed using clear resin on a Form3 printer (Formlabs, USA). To recreate a tissue-like surface inside the ear canal, a coating of silicone rubber (Dragon Skin 30, Smooth-On, USA) containing skin-coloured pigment is applied. Whilst the soft robot prototype is investigated at 2x the original scale, the ear model is 3x its original scale to accommodate for the layer thickness of the coating. A depiction of the phantom is shown in Fig. 10 b-c).

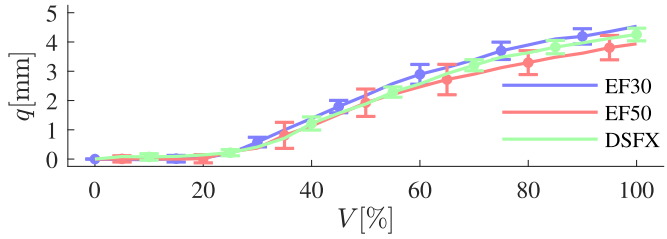

Fig. 11. Mean actuation chamber inflation q and respective standard deviation for six actuation chambers caused by induced actuation fluid volumes V for Ecoflex 00-30 (EF30), 00-50 (EF50) and Dragon Skin Fx Pro (DSFX).

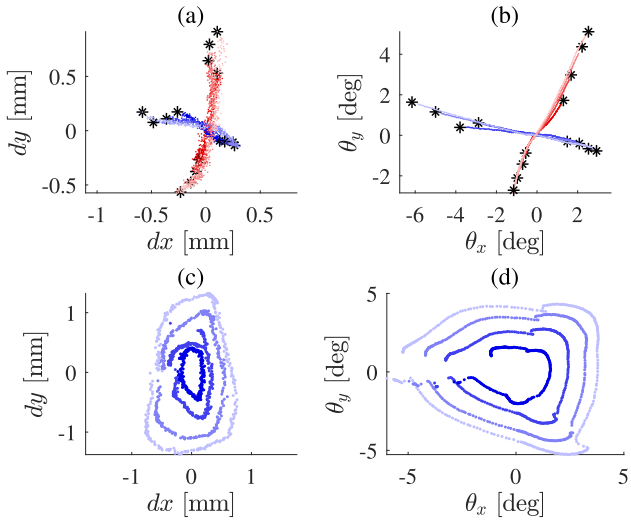

Fig. 12. Linear (a-b) and circular trajectories (c-d) in position (a,c) and orientation (b,d) at a base inflation of 75%.

III. Results

A. Actuation Characterisation

The resulting volume-inflation curves are presented in Fig. 11 for the respective materials. The induced fluid volume is expressed as a percentage of the maximum volume which is found experimentally as the limit prior to breakage as 0.57 ml.

For all materials a deadband is observable which ranges up to $\approx 20\%$ inflation. This is in-line with findings from previous work [18] for a hydraulic soft robot. The subsequent inflation profile follows a monotonic increase, which flattens for larger volumes. For the three prototypes, the maximum inflations for the given fluid volume is with 4.85 mm, 4.47 mm and 4.58 mm similar. Thus, it can be concluded that the prototypes can, on average, expand from a diameter of 8 mm to 17.27 mm when no external contact is present.

B. Steering Capabilities

Linear trajectories along x_{ctr} and y_{ctr}, are defined, ranging from ± 1 mm in 0.5 mm increments to ± 2.5 mm. The resulting robot motions are presented in Fig. 12 a). Similarly, tilting of the

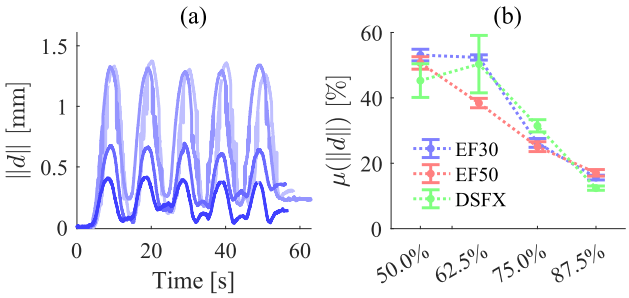

Fig. 13. Needle displacement magnitude $\|d\|$ as observed for varying inflation levels of the soft robot fabricated from Ecoflex 00-30 (a). Resulting trend for mean peak displacement relative to the reference motion for all three prototypes (b).

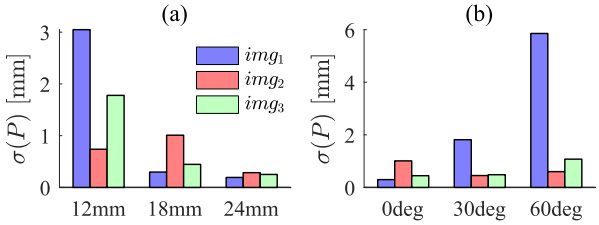

Fig. 14. Target point deviation over distance to tympanic membrane (a) and tilt with camera (b).

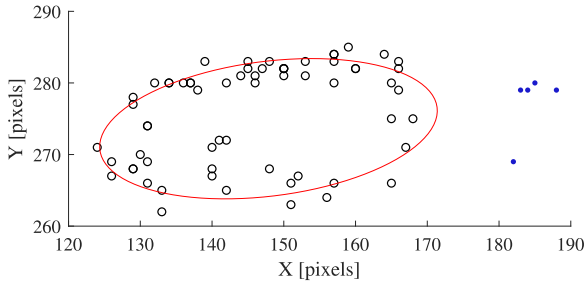

Fig. 15. Motion of insertion point in the camera frame for soft robot performing circular rotation motion inside the phantom. Outliers are highlighted in blue.

robot is shown for rotations about x_{ctr} and y_{ctr}, θ_x and θ_y, for demanded poses of ± 7.5 deg to ± 15 deg in 2.5 deg increments. Results are shown in Fig. 12 b). For both cases, translation and tilting, circular trajectories are performed for radii ranging from 1 mm to 2.5 mm in 0.5 mm increments and 7.5 deg to 15 deg in 2.5 deg increments respectively, which are shown in Figs. 12 c)-d). To allow for easier comparison, trajectories are centred around their centrepoint.

Across all trajectories, the generated motion is lower when compared to the demanded trajectory of the simplified kinematics model, which is caused by the interaction between soft actuators and environment. For the given initial inflation of 75% this reduces the total steering motion distance to 0.47 mm, 0.61 mm, 0.89 mm and 1.03 mm in x and 0.84 mm, 1.04 mm, 1.29 mm and 1.52 mm in y. The respective increment is 0.19 ± 0.08mm in x and 0.23 ± 0.03mm in y. Similarly, the resulting tilts are lower with 4.46°, 5.98°, 7.75° and 9.4° in x and 3.21°, 5.09°, 7.34° and 8.76°. It can be seen that the resulting trajectory increment is $1.65 \pm 0.13°$ in x and $1.85 \pm 0.42°$ in y.

Whilst the magnitude of the motion is lower, the direction is predictable and consistent across trials. The rate with which the range of the trajectory increases is consistent and thus allows for compensation when the coupling state is known. The targeted directions of the line segments in x and y are mostly perpendicular with an average angle of 99.64° between them.

For circular trajectories a difference of 0.39 ± 0.15 mm in translation and $2.12 \pm 0.39°$ in rotation between start and end pose is noticeable. This could be caused by frictious sliding motion between inflated actuators and acrylic tube as well as hysteresis in the material.

C. Motion Compensation

The soft robot is stabilised within the acrylic tube and offset inflation levels of 50%, 62.5%, 75% and 87.5% are applied. The needle is fixed to the robotic manipulator and inserted with a distal length of 40 mm being free. The total needle length is 87 mm. The manipulator generates displacements of 2.5 mm, which are repeated five times. The resulting needle motions are presented in Fig. 13 for the four inflation levels relative to the unconstrained needle motion. Time series indicating the motion magnitudes ($\|d\|$) are shown in Fig. 13 a) for EF30. The mean maximum motion corresponding to the peaks of all time series are shown in Fig. 13 b). All three prototypes reduce the induced needle motion efficiently with increasing inflation level. The motion is in most cases monotonically reduced with low variability. Only in case of DSFX, the motion increases slightly after the initial inflation, which could indicate slippage in the contact between robot and tube. At 87.5% the stiffer DSFX is able to reduce the motion the furthest to $12.39 \pm 0.66\%$ compared to $15.63 \pm 0.73\%$ for EF30 and $17.07 \pm 1.00\%$ for EF50.

D. Target Identification and Tracking

Target tracking performance is evaluated for the target distances 12 mm, 18 mm and 24 mm at 0° tilt between camera and image plane. Tilt angles of 0°, 30° and 60° between camera and image are evaluated at a distance of 18 mm. The recorded standard deviation of the target location P is shown in Fig. 14 for distance (a) and tilt (b). It can be seen that variability in the target location drops on average with the distance to the image, which could be caused by only a smaller region of the membrane being visible for smaller distances. The tilt angle also impacts target variability drastically, particularly for image 1. The effect is lower for images 2 and 3.

The tracking performance of the insertion point with the camera being integrated into the soft robot is shown in Fig. 15 for a circular robot trajectory. The resulting elliptical path of the tracked insertion points is highlighted in red. It can be seen that despite some variability in the position retains tracking across the motion.

IV. Discussion

The here-presented system is a first proof-of-concept of a soft robot comprising radial directed radial inflation within a lumen. It has been shown that the soft robot can inflate substantially and

increase its diameter to $\approx 216\%$. Extrapolating to the original scale of the procedure, it can be assumed that a robot of 4 mm diameter is able to adapt to and stabilise itself inside an ear canal of 7 mm while still retaining enough actuation range to allow for efficient steering. The workspace of the system can be increased by shortening the distance between both actuation stages as well as by reducing the diameter of the core. A resulting decrease in core stiffness could be addressed by choosing materials with greater shore hardness. Whilst the obtained results indicate low variability in the inflation characteristics of individual actuators, the remaining drive system is susceptible to variations through entrapped air and other external factors which affects the robot's output motion. Hence online calibration methods should be developed to compensate for occurring variability during the procedure.

The soft robot's workspace is determined by inflation of individual actuators. Extrapolating from the here-presented results in that can be assumed that there is a physical limit of inflation the ballooning actuators approach with increasing fluid volume. Thus, relying on the membranes alone can limit the steering capabilities if greater robot motion ranges are required. To further increase the workspace of the proposed system, methods of reducing non-radial expansion will be investigated. This could include fibre- or spring-reinforcements and meshes amongst others.

The soft robot is able to significantly reduce needle motion during insertion for all three investigated prototypes. It can be seen that whilst the stiffness of the material does not play a significant role in the reduction, at the maximum investigated inflation the stiffest prototype (DSFX) can reduce the needle motion the furthest. Investigations have to be conducted to determine the resulting stress variation in the tympanic membrane, the effect of the placement of the robot along the ear canal as well as the resulting pain perception in the patient.

An investigation into the stiffness behaviour of the system needs to be conducted to be able to accurately model the systems motion under external contacts. As it has been shown in previous work, it is possible to relate forces acting on a fluid-driven soft robot to internal hydraulic pressure variations [20]. This methodology could be employed to maximise comfort in the patient by actively controlling the clamping force of the system.

V. Conclusion

We have presented the first prototype for a novel soft robot with the aim to de-risk intratympanic injections by enabling active steering of the inserted needle with the help of a vision system and potentially reduce pain in patients by compensating undesired needle motion during the procedure. We have presented the design, established a highly-scalable fabrication method and created a number of prototypes with varying degrees of stiffness. The embedded fluid actuators have shown consistent inflation characteristics, capable of anchoring and steering the robot within a lumen twice its diameter. The robot is able to follow linear and circular trajectories in Cartesian space, which lays the basis for future investigations into closed-loop control of the system. By the detecting the desired injection point on the tympanic membrane, the proposed vision system paves the way for image-guided control of the robot, leading to further de-risking of the procedure.

References

[1] F. Piu and K. M. Bishop, "Local drug delivery for the treatment of neurotology disorders," *Front. Cell. Neurosci.*, vol. 13, no. 238, pp. 1–11, Jun. 2019.

[2] M. Patel *et al.*, "Intratympanic methylprednisolone versus gentamicin in patients with unilateral ménière's disease: A randomised, double-blind, comparative effectiveness trial," *Lancet*, vol. 388, no. 10061, pp. 2753-2762, 2016.

[3] M. Lechner, L. Sutton, M. Ferguson, Y. Abbas, J. Sandhu, and A. Shaida, "Intratympanic steroid use for sudden sensorineural hearing loss: Current otolaryngology practice," *Ann. Otol. Rhinol. Laryngol.*, vol. 128, no. 6, pp. 490–502, 2019.

[4] C. R. Anderson, C. Xie, M. P. Su, M. Garcia, H. Blackshaw, and A. G. Schilder, "Local delivery of therapeutics to the inner ear: The state of the science," *Front. Cell. Neurosci.*, vol. 13, p. 418, Oct. 2019. [Online]. Available: https://www.frontiersin.org/article/10.3389/fncel.2019.00418

[5] S. Atallah, B. Martin-Perez, D. Keller, J. Burke, and L. Hunter, "Natural-orifice transluminal endoscopic surgery," *Brit. J. Surg.*, vol. 102, no. 2, pp. 73–92, 2015.

[6] B. Zheng *et al.*, "Quantifying mental workloads of surgeons performing natural orifice transluminal endoscopic surgery (NOTES) procedures," *Surg. Endosc.*, vol. 26, no. 5, pp. 1352–1358, 2012.

[7] M. Arnold, M. S. Sierra, M. Laversanne, I. Soerjomataram, A. Jemal, and F. Bray, "Global patterns and trends in colorectal cancer incidence and mortality," *Gut*, vol. 66, no. 4, pp. 683–691, 2017.

[8] N. Patel *et al.*, "Evaluation of a novel flexible snake robot for endoluminal surgery," *Surg. Endosc.*, vol. 29, no. 11, pp. 3349–3355, 2015.

[9] F. Cosentino *et al.*, "Robotic Colonoscopy," in *Colonoscopy. IntechOpen*, 2011. [Online]. Available: https://www.intechopen.com/books/colonoscopy/robotic-colonoscopy

[10] L. Manfredi, E. Capoccia, G. Ciuti, and A. Cuschieri, "A soft pneumatic inchworm double balloon (SPID) for colonoscopy," *Sci. Rep.*, vol. 9, no. 1, pp. 1–9, 2019.

[11] J. O. Alcaide, L. Pearson, and M. E. Rentschler, "Design, modeling and control of a SMA-actuated biomimetic robot with novel functional skin," in *Proc. IEEE Int. Conf. Robot. Automat.*, 2017, pp. 4338–4345

[12] N. Gluck, A. Melhem, Z. Halpern, K. Mergener, and E. Santo, "A novel self-propelled disposable colonoscope is effective for colonoscopy in humans (*with video*)," *Gastrointest. Endosc.*, vol. 83, no. 5, pp. 998–1004, 2016.

[13] B. T. Faddis, "Structural and functional anatomy of the outer and middle ear," *Anatomy Physiol. Hear. Audiologists*, W. Clark & K. Ohlemiller Eds., Thomson Delmar Learning, pp. 93–108, 2008.

[14] S. Asgari Taghanaki, K. Abhishek, J. P. Cohen, J. Cohen-Adad, and G. Hamarneh, "Deep semantic segmentation of natural and medical images: A review," 2020, Art. no. 0123456789. [Online]. Available: https://doi.org/10.1007/s10462-020-09854-1

[15] L.-C. Chen, Y. Zhu, G. Papandreou, F. Schroff, and H. Adam, "Encoder-decoder with atrous separable convolution for semantic image segmentation," in *Proc. Eur. Conf. Comput. Vis.*, 2018, pp. 801–818.

[16] M. Sandler, A. Howard, M. Zhu, A. Zhmoginov, and L. C. Chen, "MobileNetV2: Inverted residuals and linear bottlenecks," *Proc. IEEE Comput. Soc. Conf. Comput. Vis. Pattern Recognit.*, 2018, pp. 4510–4520.

[17] E. Başaran, Z. Cömert, and Y. Çelik, "Convolutional neural network approach for automatic tympanic membrane detection and classification," *Biomed. Signal Process. Control*, vol. 56, 2020, Art. no. 101734.

[18] L. Lindenroth, R. J. Housden, S. Wang, J. Back, K. Rhode, and H. Liu, "Design and integration of a parallel, soft robotic end-effector for extracorporeal ultrasound," *IEEE Trans. Biomed. Eng.*, vol. 67, no. 8, pp. 2215–2229, Aug. 2020.

[19] D. Sieber *et al.*, "Data descriptor: The openEar library of 3D models of the human temporal bone based on computed tomography and micro-slicing," *Sci. Data*, vol. 6, 2019, Art. no. 180297.

[20] L. Lindenroth, C. Duriez, J. Back, K. Rhode, and H. Liu, "Intrinsic force sensing capabilities in compliant robots comprising hydraulic actuation," in *Proc. IEEE Int. Conf. Intell. Robots Syst.*, Vancouver, BC, Sep. 2017, pp. 2923–2928, doi: 10.1109/IROS.2017.8206125.